Marine Geology 464 (2023) 107148

Contents lists available at ScienceDirect

Marine Geology

journal homepage: www.elsevier.com/locate/margo

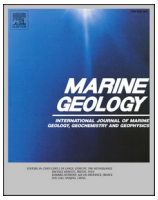

Research Article

Consequences of limited sediment supply for long-term evolution of offshore tidal sand waves, a 3D model perspective

A. Nnafie *, J.M. Krabbendam, H.E. de Swart

Institute for Marine and Atmospheric research, Utrecht University, Utrecht, the Netherlands

ARTICLE INFO

Editor: Shu Gao

Keywords:
3D morphodynamic model
Tides
Sediment transport
Sediment-starved conditions
Shape
Spacings
Height
Migration

ABSTRACT

Field data show that offshore tidal sand waves in areas where sediment supply is limited have different characteristics (shape and dimensions) compared with their counterparts in areas with sufficient sediment supply. So far, only the initial formation of tidal sand waves on a sediment-starved shelf has been studied with a 2DV model that ignores variations along the crests. In this study, a 3D non-linear morphodynamic model is used to investigate the effects of sediment availability on the long-term evolution of offshore tidal sand waves. Overall, the simulated sand waves have characteristics that resemble those of observed sand waves. The mature sand waves that develop in the case of limited sediment supply (i.e., thickness of erodible sediment layer is smaller than the height of sand waves) are more three-dimensional, i.e., having isolated and more irregular crestlines compared with those in the case of sufficient supply. With decreasing sediment supply, sand waves have larger spacings between successive crests, smaller heights and they migrate faster. These differences in the characteristics of the sand waves start to occur once the hard bed underneath the erodible sediment layer is exposed.

1. Introduction

Offshore tidal sand waves (also called "tidal dunes", Van Landeghem et al., 2009; Ma et al., 2019) are rhythmic bedforms with mean spacings between successive crests of several hundreds of meters, heights (crest-to-trough distance) of a few meters, migration speeds up to tens of meters (Van Veen, 1935; McCave, 1971; Zhou et al., 2022; Van der Meijden et al., 2023) and crests that are oriented almost perpendicular to the direction of the main tidal current (Besio et al., 2008). They are observed on the sandy bed of many shallow continental shelf seas, such as that of the North Sea, the Gulf of Cadiz (Lobo et al., 2000), the Irish Sea (Van Landeghem et al., 2009), the coastal waters of Japan (Katoh et al., 1998) and Canada (Duffy and Hughes-Clarke, 2005). Due to their dynamic nature, tidal sand waves may pose a hazard to offshore human activities by, e.g., infilling navigation channels, exposing buried electricity cables and pipelines in the sea bottom and damaging wind mill parks (Dorst et al., 2011).

Field data show that the characteristics (shapes and dimensions) of sand waves that form in areas with sufficient sediment availability (i.e., the thickness of erodible sediment layer d is larger than the maximum height of sand waves H_{max}, $d > H_{max}$) differ from those that are found in sediment-starved areas where availability of erodible sediment is limited ($d < H_{max}$). For example, Flemming (1980) reported the presence of a field of sand waves in a sediment-rich environment on the continental shelf of South Africa, which were two-dimensional (2D), i.e., with almost straight crestlines. In sediment-starved areas on this shelf, three-dimensional (3D) sand waves were observed, which were characterized by more meandering crestlines and larger spacings between successive crests compared with their counterparts in sediment-rich areas. Similar bottom patterns were observed by Le Bot and Trentesaux (2004) in the Dover Strait (southern North Sea), who found that sand waves in sediment-starved areas were often spaced further apart, higher and more strongly 3D than those in sediment-rich areas. In the Irish Sea, field measurements (Van Landeghem et al., 2009) revealed that the growth of bedforms was weaker in sediment-starved areas than in sediment-rich areas. Based on field data on the Belgian continental shelf, Krabbendam et al. (2022) hypothesized that the observed differences between the morphodynamic response of tidal sand waves to dredging in the different areas were caused by the differences in the availability of erodible sediment in each of these areas.

A process-based modelling study into the effects of supply-limited conditions on the morphodynamics of tidal sand waves was conducted by Porcile et al. (2017). Their model results showed that under sediment supply-limited conditions, sand waves have larger spacings between

* Corresponding author.
E-mail address: a.nnafie@uu.nl (A. Nnafie).

https://doi.org/10.1016/j.margeo.2023.107148
Received 21 March 2023; Received in revised form 13 September 2023; Accepted 19 September 2023
Available online 23 September 2023

successive crests and they have sharp crests and flat troughs compared with those that form under supply-unlimited conditions. This model was highly idealised, in the sense that, first, it was 2DV, i.e., it assumed conditions along the crests of the sand waves to be spatially uniform. Second, the hydrodynamics were computed under the assumption that the amplitude of bed elevations is much smaller than the water depth and thus they did not represent sand waves during their phase after initial formation.

The preceding considerations motivated the overall objective of this study, which is to gain an understanding of the observed changes in the degree of three-dimensionality of sand waves under increased sediment-starved conditions. Clearly, this requires a 3D model, which has not been used in this context. The specific objective is to quantify the effects of sediment availability on the characteristics (the degree of three-dimensionality, spacing between successive crests, height, migration speed) of the sand waves. To this end, a 3D morphodynamic model will be used to study the long-term evolution of tidal sand waves under limited supply conditions and compare their characteristics with their counterparts under sufficient supply conditions. The model setting (domain and parameter values) is identical to one of the settings of the 2DV model used by Krabbendam et al. (2021), the main difference being the addition of the third dimension. This choice was made because Krabbendam et al. (2021) successfully calibrated and validated their model against observed sand waves in four different areas in the North Sea.

Section 2 describes the morphodynamic model, as well as the design of experiments and the methods to analyse the sand wave characteristics. Results are presented in Section 3 and discussed in Section 4. The conclusions are given in Section 5.

2. Material and methods

2.1. Model description

In this study, the Delft3D model (Lesser et al., 2004) is employed, which solves equations for flow, sediment transport and bed evolution in (X, Y, σ)-coordinates (Lesser et al., 2004). Here, (X, Y) are the co-ordinates along the two horizontal directions, with dimensions $L_X \times L_Y$ (Fig. 1a) and $\sigma = \frac{z-\eta}{D}$ is a sigma coordinate, with z the vertical coordinate (with $z = 0$ the mean sea level) and η the water level with respect to $z = 0$. Furthermore, $D = -z_b + \eta$ is the total water depth, with $z_b = -H_0 + h$, H_0 the undisturbed water depth and h the bed perturbations with respect to the initial bed level ($z_{b0} = -H_0$). Value of σ at the bed ($z = z_b$, with z_b the bed level) is $\sigma = -1$ and at the free surface ($z = \eta$), $\sigma = 0$. A high-resolution area (with dimensions (ℓ_X, ℓ_Y)) is defined in the centre of the model domain (hereafter referred to as the area of interest), which is necessary to accurately resolve the sand wave dynamics. The currents are computed by solving the 3D-shallow water equations, thereby using the $k - \varepsilon$ turbulence closure model to calculate the vertical eddy viscosity. Furthermore, a uniform bed roughness is assumed, with roughness length k_s. The computed currents are subsequently used to calculate bedload ($\vec{q}_b$) and suspended load transport ($\vec{q}_s$) using the formulations of Van Rijn (1993). The sediment transport is computed from the skin friction, which is the part of the total bed-shear stress that acts on the

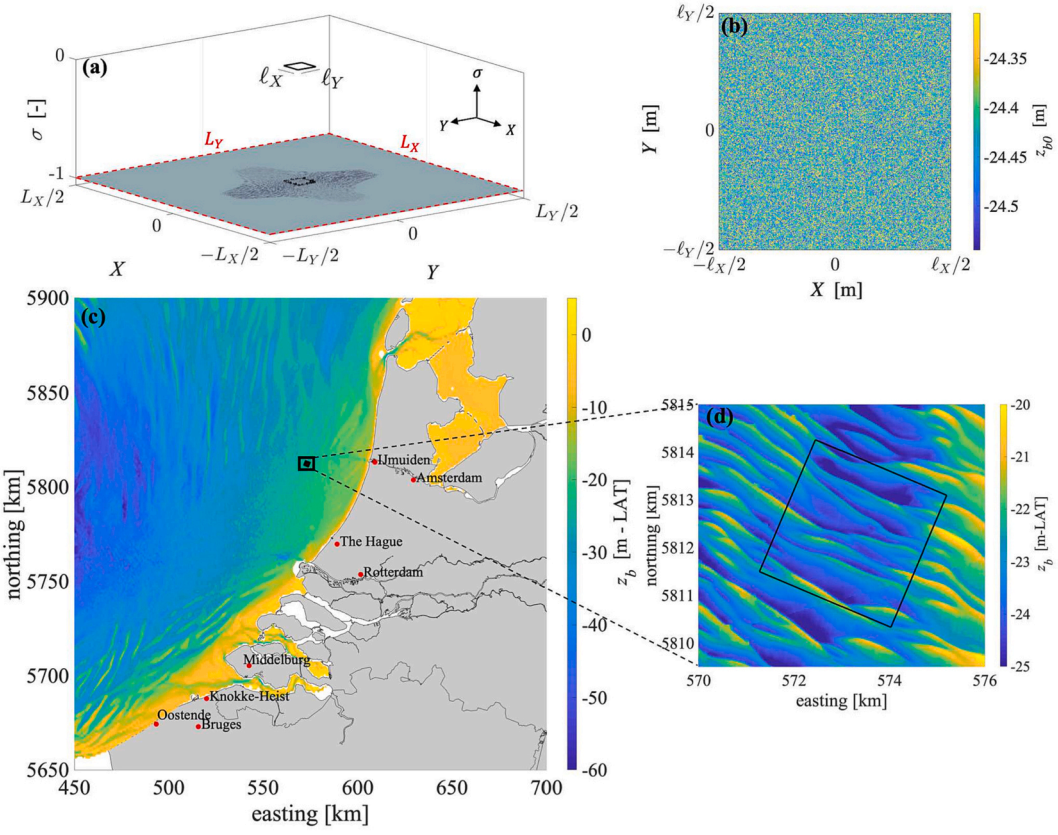

Fig. 1. (a) Model domain in (X, Y, σ)-coordinates, with horizontal lengths L_X and L_Y, and the scaled vertical coordinate σ (-1 at the bottom, 0 at the free surface). The red, dashed lines denote the location of the open boundaries and (ℓ_X, ℓ_Y) correspond to the part of the domain with the highest horizontal resolution referred to as the area of interest. (b) Initial bed level $z_{b0}(X, Y) = -H_0$ (H_0 is the undisturbed water depth) in the area of interest, with superimposed random, small-amplitude bed perturbations that are used to initiate model simulations. c) Bathymetric map of the North Sea in the year 2020, which was constructed using the EMODnet bathymetry portal (http://portal.emodnet-bathymetry.eu/). d) Zoom-in on a field of sand waves (Netherlands Hydrographic Service, 2017), on which model parameters were based. The degree of three-dimensionality (f_{3d}) of this sand wave field is about 0.7. (For interpretation of the references to colour in this figure legend, the reader is referred to the web version of this article.)

sediment particles. Further details are given in Van Rijn (1993). Bedslope-induced sediment transport is accounted for in both the direction of local flow and in the direction perpendicular to that, with bedslope coefficients α_{BS} and α_{BN}, respectively. Bed level $z_b(X, Y, t)$ is dynamically updated as a result of 1) the net sediment exchange between the sea bed and the overlying water column and 2) the divergence/convergence in the bedload sediment transport.

At the open boundaries ($X = -L_X/2$, $X = L_X/2$, $Y = -L_Y/2$, $Y = L_Y/2$), denoted by the red, dashed lines in Fig. 1a, combined tidal water levels and depth-averaged tidal velocities are imposed using the weakly reflective Riemann invariants R. The latter are defined in terms of sea surface height and depth-averaged currents. It is moreover assumed that at these boundaries, the profile of the velocity over the vertical is logarithmic. Furthermore, equilibrium concentration profiles are prescribed at the open boundaries, by assuming a balance between sediment settling and sediment erosion.

2.2. Handling limited sediment availability

The model assumes a non-erodible bed underneath the erodible sediment layer. When the non-erodible sediment layer is exposed at a particular location by erosion, there is no entrainment of sediment in the water column, causing sediment starvation at this location. This lack of erodible sediment is managed in the model by reducing the magnitudes of bed-load and suspended load transports (q_b and q_s, respectively) at this location by a factor of d/d_c, as soon as the thickness of the erodible sediment layer (d) drops below a user-specified critical layer thickness (d_c). These transports vanish when the non-erodible layer is fully exposed ($d = 0$).

2.3. Model configuration

Values of the model parameters presented in this section are based on an area in the Dutch North Sea that features the presence of tidal sand waves (Fig. 1c and d). This area, which is characterized by abundant erodible sediment, is selected because 1) of its large availability of data and that 2) an earlier 2DV version of the model has proven to be successful in simulating the observed evolution of sand waves in this area during the period 1999–2012 (Krabbendam et al., 2021). A model domain with horizontal dimensions of $L_X \times L_Y = 40 \times 40$ km^2 is used. Horizontal grid spacings are $(\Delta X, \Delta Y) = (590, 590)$ m at the model boundaries and they decrease to $(\Delta X, \Delta Y) = (10, 10)$ m in the area of interest, which has dimensions $\ell_X \times \ell_Y = 3 \times 3$ km^2 (Fig. 1a and b). The use of this high resolution inside the area of interest is needed to accurately resolve the sand wave dynamics (Krabbendam et al., 2021). The water column is divided into 30 non-equidistant σ-layers, whose thicknesses increase from bottom to surface. The first five layers above the bed each have thicknesses $< 1\%$ of the total water depth, while the last five layers have thicknesses of $\sim 6\%$ of the water depth. A spatially uniform initial bed level $z_{b0} = 24.4$ m is assumed, with superimposed random bed perturbations $h(X, Y)$ with an amplitude of 10 cm in the area of interest (Fig. 1b). The amplitude of these perturbations, which are generated with the white-noise function of MATLAB, decreases gradually to zero outside of the area of interest.

To derive water levels and depth-averaged velocities at the model boundaries ($X = -L_X/2$, $X = L_X/2$, $Y = -L_Y/2$, $Y = L_Y/2$), the model is nested in the calibrated tidal North Sea model DCSM-ZUNO (for further details see Zijl et al., 2015). The water levels and velocities are combined into Riemann M_2, M_4, M_6 and M_0 amplitudes and phases, which are subsequently imposed at the model boundaries. Here, M_2 refers to the semi-diurnal lunar tide, M_4 and M_6 are overtides and M_0 is the residual component. The roughness length k_s is based on the dimensions of megaripples in the study area. Using the formulation of Van Rijn (1993), this yields a value of $k_s = 0.1$ m. One single median grain size with diameter d_{50} of 285 μm is considered (Damen et al., 2018). Following Van Gerwen et al. (2018), the longitudinal and transverse bedslope coefficients are set to $\alpha_{BS} = 3$ and $\alpha_{BN} = 1.5$, respectively. The time step Δt is 12 s. To reduce computation time, a MORFAC (morphological acceleration factor) of 2000 is applied. This is justified because the morphodynamic evolution of the sand waves takes place on much longer time scales (order of decades) than the hydrodynamic evolution (order of hours and days). Test experiments reveal that using smaller values of MORFAC does not yield different results. The critical layer thickness is set to $d_c = 5$ cm.

2.4. Model experiments

To address the objective of this study, three numerical experiments are conducted with different initial thicknesses δ of the erodible sediment layer: (1) $\delta = 25$ m (referred to as unlimited supply), (2) $\delta = 1$ m and (3) $\delta = 0.5$ m. The bed below these erodible sediment layers is a motionless substratum. Each of the three experiments starts with the same initial bed perturbations. Moreover, the first two tidal cycles are used for spin-up, during which no bed level changes take place. Each experiment is carried out for a maximum simulation time of 275 years, which takes about three months on an Intel Xeon 2.10 GHz Linux computer. Note that, due to these long computation times, the number of experiments is limited to three.

2.5. Analysis of model output

Preliminary model results show that crests of elongated sand waves are, overall speaking, perpendicular to the main depth-averaged current. To facilitate the analysis of model results obtained from the three experiments, a new coordinate system (x,y) is defined, with x pointing in the direction of the main depth-averaged tidal current and y in the direction perpendicular to that, so approximately aligned with the crestlines of the sand waves. The new x,y-axes are obtained by rotating the original X, Y-axes by 13° in the anti-clockwise direction (Fig. 2a). The new bed level $z_b(x_m, y_n)$ is obtained by a linear interpolation of the original bed level on the new grid (x_m, y_n). Here, $m = 1, \ldots, N_n$ and $n = 1, \ldots, N_m$, with N_n and N_m the number of grid points in the x and y direction, respectively. Note that N_m and N_n are not constants, because of the applied rotation of the domain. The new and old grids have the same resolution. Positions of a crest and its adjacent trough of a sand wave are indicated by index p ($p = 1, \ldots, P$, with P the number of sand waves in the area of interest, Fig. 2b). Applying a more sophisticated interpolation method (cubic) does not affect the results.

Data of bed levels are analysed as follows. First, the degree of three-dimensionality of the sand waves f_{3d} is defined as

$$f_{3d} = \frac{\sigma_{3d}^2}{\sigma_{3d}^2 + \sigma_{2d}^2}. \tag{1}$$

Here, σ_{2d}^2 is the variance of $z_{b,2d}(x_m)$, with the latter being the average value of bed level $z_b(x_m, y_n)$ along transect $x_m =$ constant, i.e.,

$$z_{b,2d}(x_m) = \frac{1}{N_m} \sum_{n=1}^{N_m} z_b(x_m, y_n). \tag{2}$$

The quantity σ_{3d}^2 indicates the variance of bed level difference $z_b'(x_m, y_n) = z_b(x_m, y_n) - z_{b,2d}(x_m)$. These variances are computed using the following expressions:

$$\sigma_{2d}^2 = \frac{1}{N_{n,max}} \sum_{m=1}^{N_{n,max}} \left(z_{b,2d}(x_m)\right)^2, \tag{3}$$

$$\sigma_{3d}^2 = \frac{1}{N_{3D}} \sum_{n=1}^{N_m} \sum_{m=1}^{N_n} \left(z_b'(x_m, y_n)\right)^2, \tag{4}$$

where $N_{n,max}$ is the maximum number of transects $x_m =$ constant and N_{3D}

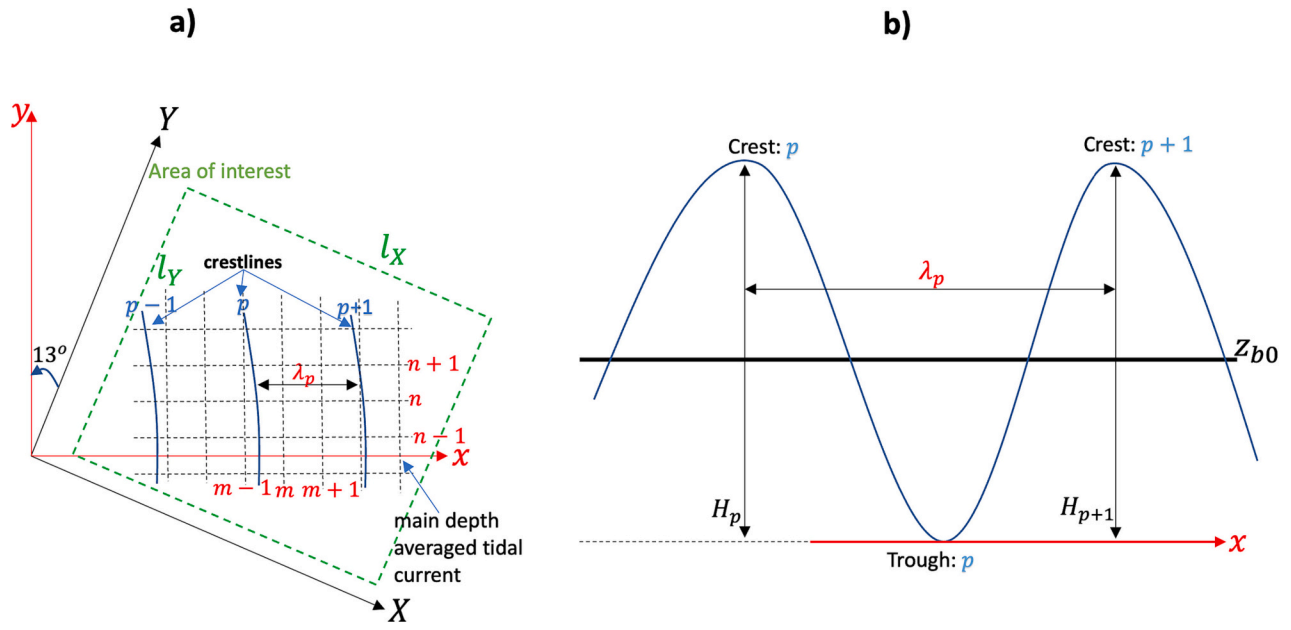

Fig. 2. (a) View of the new coordinate system (x,y), with the x-axis pointing in the direction of the main depth-averaged tidal current and the y-axis perpendicular to that. The new coordinate system is obtained by rotating the original X,Y-axes by 13° in the anti-clockwise direction. Indices m ($m = 1,\ldots,N_n$) and n ($n = 1,\ldots,N_m$) denote the labels of the grid points in the x and y directions, respectively. Here, N_n and N_m are the number of grid points along transects y_n = constant and x_m = constant, respectively. Crests and troughs of the sand waves are indicated by indices p ($p = 1,\ldots,P$, with P the number of sand waves in the area of interest). Spacing λ_p is the horizontal distance measured along the x-axis between two successive crests with indices p and $p+1$. b) Sketch of a sand wave crest and its adjacent trough along the x-axis. Height H_p is defined as the vertical distance between a crest and its adjacent trough of the sand wave with index p.

is the total number of grid points in the area of interest. The value of f_{3d}, which lies between 0 and 1, quantifies to what extent the full bed level $z_b(x_m,y_n)$ can be approximated by $z_{b,2d}(x_m)$. A value f_{3d} close to 0 means that σ^2_{2d} is large compared to σ^2_{3d} and most of the bed level variance is captured by $z_{b,2d}$. In this case, the sand waves are considered to be fully two-dimensional (2D). When f_{3d} approaches 1, most of the bed level variance is in $z_b(x_m,y_n)$ (i.e., $\sigma^2_{3d} \gg \sigma^2_{2d}$) and the bedforms are regarded as fully three-dimensional (3D). Bedforms with an increasing (decreasing) f_{3d} are said to become more (less) 3D. Finally, note that f_{3d} in Eq. (1) is a new metric that has been introduced in the present study to quantify the three-dimensionality of an entire sand wave field. Previous studies (Rubin, 2012; Núñez-González et al., 2021) used other metrics to quantify the degree of three-dimensionality, but these metrics described individual sand waves, rather than an entire sand wave field.

Second, the mean spacing of the sand waves is defined in the direction of the main depth-averaged tidal current (x-axis). Here, the spacing of a sand wave (λ_p) represents the horizontal distance between two successive crests with indices p and $p+1$, which is measured along the x-axis (Fig. 2b). The mean spacing (indicated by $[\lambda_x]$) is computed by averaging over all individual spacings λ_p.

Third, mean heights $[H]$ (crest-to-trough distance along transects along the x-axis, Fig. 2b) of the sand waves are determined following the same procedure as that to compute $[\lambda_x]$.

Finally, the migration speed V_m, which is defined as the rate at which the sand waves propagate in the x-direction, is estimated based on the slope of the crestlines in the (x,t) domain, dx/dt, with t time. To this end, bed level profiles $z_b(x,y=0)$ along transect $y=0$ are plotted in the (x,t) domain.

3. Results

Fig. 3 shows two snapshots of bed level $z_b(x,y)$ at times $t = 150$ yr and $t = 220$ yr. Here, the rows represent different initial sediment thicknesses and the left and right columns correspond to, respectively, times $t = 150$ yr and $t = 220$ yr. In all cases, mature tidal sand waves

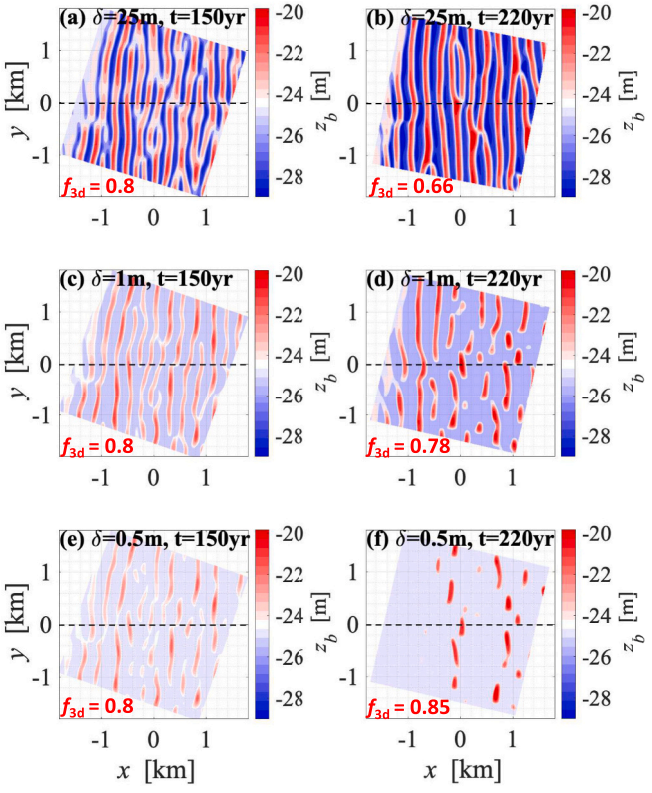

Fig. 3. Snapshots of bed level $z_b(x,y)$ at times $t = 150$ years (left columns) and $t = 220$ years (right columns) for layer thickness $\delta = 25$ m (a-b), $\delta = 1$ m (c-d) and $\delta = 0.5$ m (e-f). The dashed black lines denote the transects used in Fig. 5. Degree of three-dimensionality f_{3d} is also shown (in the bottom left of each panel).

develop on a time scale of decades. Overall, these snapshots show that, in the case of sufficient sediment availability ($\delta = 25$ m), elongated and more regularly-spaced tidal sand waves develop across the domain, while those that form in the cases of smaller layer thicknesses have more irregular and three-dimensional planforms. Particularly in the case of $\delta = 0.5$ m, the sea bottom eventually features the presence of rather small-scale and isolated mature sand waves. This difference between the sand wave patterns of the different cases is also reflected in the time development of the degree of three-dimensionality f_{3d} of the sand waves shown in Fig. 4. While in the case of sufficient supply, f_{3d} keeps on decreasing until it reaches 0.5 towards the end of the simulation, f_{3d} in the cases of limited supply increases in time, reaching values of ~ 0.8 and ~ 0.85 for $\delta = 1$ m and $\delta = 0.5$ m, respectively. This difference in the behaviour of f_{3d} arises once the hard bed beneath the erodible sediment layer is uncovered for the first time (around $t \sim 100$ yr).

Similar to the behaviour of f_{3d}, differences in the mean spacing $[\lambda_x]$ of the sand waves and their mean heights between the different cases start to occur after the hard bed is exposed (Fig. 4, panels b-c). While the mean spacing $[\lambda_x]$ of the sand waves that evolve in the case of sufficient supply ($\delta = 25$ m) remains more or less constant over time at a value of ~ 250 m, $[\lambda_x]$ increases to about 400 m and 850 m in the cases of $\delta = 1$ m and $\delta = 0.5$ m, respectively. The increase in $[\lambda_x]$ for decreasing values of δ can also be seen in Fig. 5, which displays the time evolution of bed level profiles z_b in the (x, t) domain (along transect $y = 0$, indicated by the black dashed lines in Fig. 4). In the case of $\delta = 25$ m, the sand wave height initially grows exponentially in time (panel c), eventually saturating to values of $[H] \sim 7$ m. As soon as the hard bed is uncovered in the supply-limited cases, growth (i.e., rate at which height changes with time) of the sand waves weakens, leading to the formation of smaller heights. Interestingly, in the cases of limited supply conditions ($\delta = 1, 0.5$ m) heights of the sand waves keep on increasing in time, without showing any tendency towards saturation. Moreover, the sand waves that develop in these cases have bump-shaped crests that are separated by a flat motionless substratum, particularly in the case of $\delta = 0.5$ m (see also Fig. 3f).

From Fig. 5 it appears that the slope of the crestlines of the sand waves in the (x, t)-plane, dx/dt, which is a measure for the migration speeds V_m of these bedforms, tends to become less steep with decreasing layer thickness δ. This means that sand waves migrate faster in the case of limited sediment availability. In the case of $\delta = 25$ m, sand wave migration is $V_m \sim 4$ m/yr, while in the cases of $\delta = 1$ m and 0.5 m, $V_m \sim 6$ m/yr and ~ 8 m/yr, respectively. Similar to the other sand wave characteristics, these changes in migration speed start to appear after the non-erodible layer is exposed.

Finally, note that in the case of $\delta = 0.5$ m, the results are only shown up to $t \sim 220$ years. For larger times, the mature sand waves start to migrate out of the area of interest, as a result of their larger migration speeds compared with the cases of thicker sediment layers. As the resolution outside the area of interest is not sufficient to accurately resolve the sand wave dynamics, results are disregarded for $t > 220$ years.

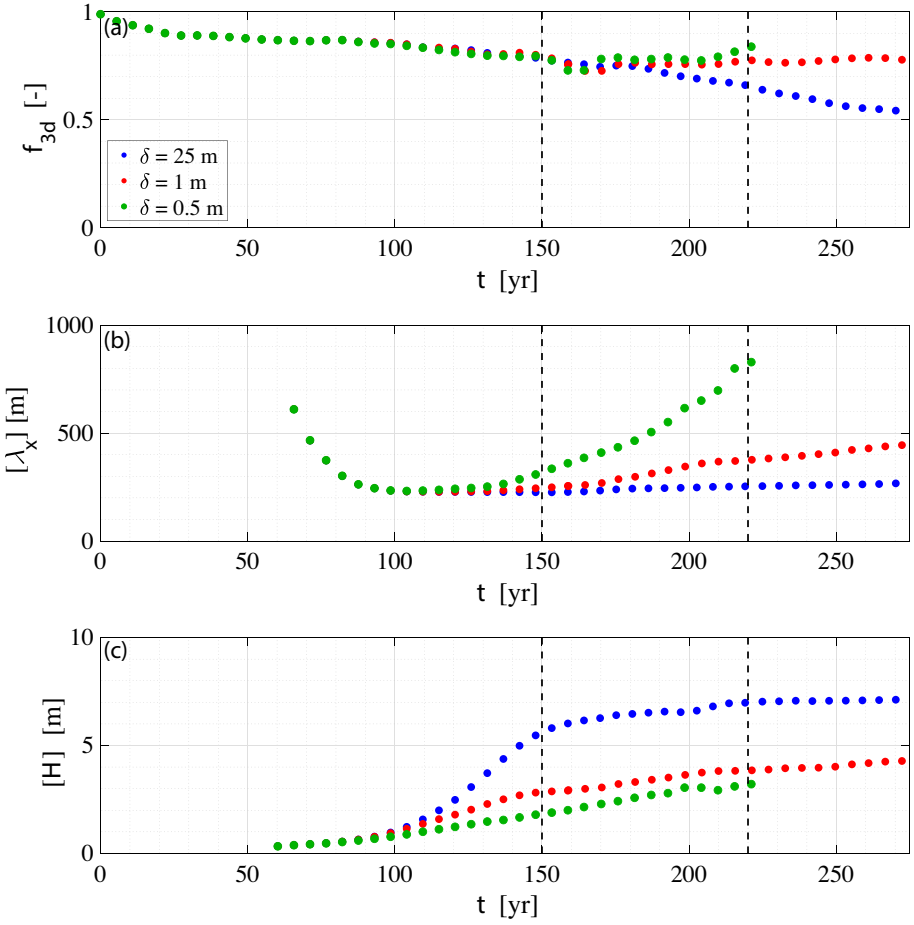

Fig. 4. Time evolution of a) the degree of three-dimensionality f_{3d}, b) domain-averaged wavelengths $[\lambda_x]$ and (c) the domain-averaged sand wave heights $[H]$ in the cases of an initial sediment layer thickness $\delta = 25$ m (blue), $\delta = 1$ m (red) and $\delta = 0.5$ m (green). The black dashed lines denote the times at which snapshots of the bed level in Fig. 3 were taken. Note that in the case of $\delta = 0.5$ m (green), the sand waves start to migrate out of the area of interest for $t > 220$ years. Results after this time are disregarded in the analysis. (For interpretation of the references to colour in this figure legend, the reader is referred to the web version of this article.)

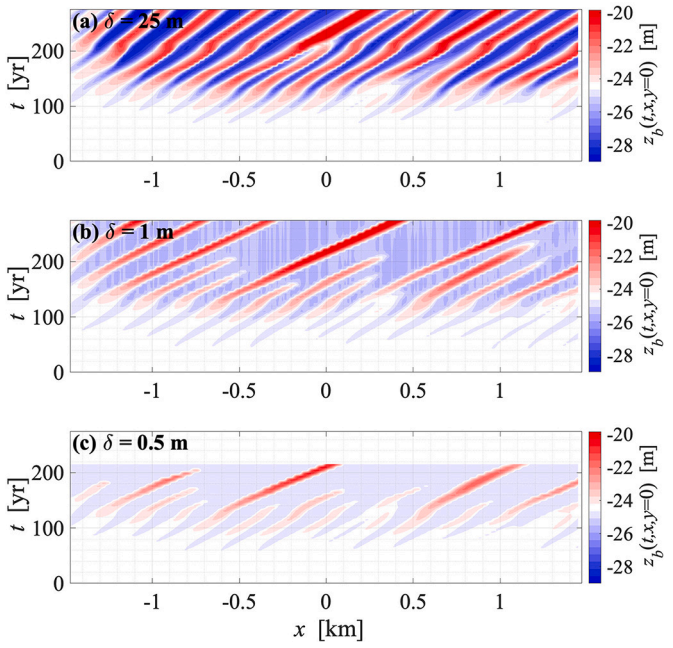

Fig. 5. Bed level $z_b(x, y = 0, t)$ (m) in the (x, t) plane along the transects depicted in Fig. 3 (black dashed lines) for layer thickness $\delta = 25$ m (a), 1 m (b) and 0.5 m (c). Red and blue colours correspond to crests and troughs, respectively. (For interpretation of the references to colour in this figure legend, the reader is referred to the web version of this article.)

4. Discussion

4.1. Comparison with previous studies

The overall aim of this study was to gain fundamental understanding of the observed changes in 3D characteristics of tidal sand waves under limited sediment-supply conditions. For this, a 3D state-of-the-art morphodynamic model was used. The methodology follows that of Blondeaux et al. (2016), the differences being that in the latter study sand ripples (here: sand waves) were investigated in a thin layer of sediment with a 2DV model (here: a 3D model). Furthermore, the present study extends that of Porcile et al. (2017), who investigated the effect of limited sand supply on the initial evolution of tidal sand waves (here: also the long-term evolution) with a 2DV model (here: a 3D model). The present study focused on general changes in the characteristics of sand waves when decreasing sediment availability. A study area with abundant erodible sediment was selected for which a 2DV version of the model was able to hindcast the past evolution of sand waves in this area. Next, the thickness of the erodible sediment layer was decreased to investigate the changes in behaviour of sand waves under increased supply-limited conditions. A direct comparison of modelled and observed sand waves in sediment-starved areas would be a next step. However, field data for such areas do not span several decades, which as yet hampers the development of a validated model. Therefore, in the remainder of this section, only general changes in sand wave characteristics when decreasing sediment availability are discussed and compared with previous studies.

Model results showed that in the case of sufficient sediment supply, the sand wave patterns become less 3D, having more regularly spaced and elongated crestlines. In contrast, in the case of limited supply, the sand waves exhibit more 3D planforms, which are characterized by more isolated and irregular crestlines. In the case of strongly limited supply conditions, the sand waves that develop have bump-shaped crests that are separated by a flat motionless substratum. Furthermore, the sand waves in the case of limited supply have larger spacings between successive crests (measured in the direction of the main depth-averaged tidal current) compared with those in the case of sufficient supply. These differences in the bedform patterns between the two cases have been also reported by field studies (e.g. Flemming, 1980; Le Bot and Trentesaux, 2004). An increased spacing with decreased sediment supply is also consistent with the outcomes of the 2DV modelling study by Porcile et al. (2017).

Regarding the heights of the sand waves, the present results generally agree with field data (Van Landeghem et al., 2009; Ma et al., 2019). Note, however, that Le Bot and Trentesaux (2004) reported sand waves being much higher in sediment-starved conditions compared with those in sediment-rich environments. This might be explained by the fact that the former bedforms were located in much deeper water compared with the latter ones. Larger water depths allow sand waves to grow higher (Carling et al., 2000; Ma et al., 2019).

Model outcomes furthermore indicate that sand waves under supply-limited conditions migrate quicker than those that form when there is sufficient sediment supply. These outcomes cannot be verified against observations due to the lack of high-resolution repeated bathymetric surveys. Several studies (Le Bot and Trentesaux, 2004; Creane et al., 2022) reported that sand waves in sediment-starved and sediment-rich areas display differences in migration speeds and directions. However, those studies attributed these differences to differences in the hydrodynamic forcing and not to sediment availability. In this context, it would also be interesting to conduct future laboratory experiments, in which the evolution of sand waves subject to oscillatory currents is studied for different thicknesses of the erodible sediment layer. So far, such experiments have been performed for steady currents (Kleinhans et al., 2002; Tuijnder et al., 2009; Porcile et al., 2020, 2023), but studies by Tambroni et al. (2005) and Leuven and Kleinhans (2019) demonstrate the feasibility of studying bedforms generated by oscillatory currents in a lab setting.

Finally, Krabbendam et al. (2022), who investigated the recovery of sand waves at three dredging sites on the Belgium shelf, observed that only at one site the sand waves recovered within the measurement period, while sand waves did not regenerate at the other two sites. They hypothesized that this difference was caused by the lack of sediment supply at the latter two sites. Present model results, which show that growth of sand waves is weaker with decreasing sediment availability, provides support for this hypothesis.

4.2. Remarks about the model

As was stated in the introduction and in Section 2.3, the 3D model has been configured such that it resembles that of the validated 2DV model of Krabbendam et al. (2021). This suggests that the 3D model contains the essential ingredients to study the effects of sediment availability on the long-term evolution of tidal sand waves. According to previous studies (e.g., Le Bot and Trentesaux, 2004; Van Gerwen et al., 2018; Campmans et al., 2018a, 2018b; Damveld et al., 2020) other aspects (e.g., wind forcing, waves, mixture of different sediment sizes, etc.), which are absent in this model, do affect the characteristics of sand waves (growth, migration, height and spacings). However, given the successful validation presented in Krabbendam et al. (2021), their effects are expected to be minor.

Finally, values for grid size, time step and MORFAC were optimized such that the computation times were not too long and that model results were still sufficiently accurate. Results from additional simulations for smaller values of grid size, time step and MORFAC (not shown) showed that smaller values did not qualitatively affect the outcomes from the present study.

4.3. Novelty of the model and its potential applications

The novelty of the present model is that it is able to simulate the 3D non-linear evolution of tidal sand waves. It is encouraging to see that a process-based complex model is able to simulate sand waves with

characteristics that resemble those of observed sand waves.

Thus, the model could be used as a tool to study, e.g., the morphodynamic response of sand waves to dredging, which may help design more cost-efficient dredging policies. Such a study would be relevant in the context of the ongoing increase of offshore human activities (construction of windmills, drilling platforms, navigation channels, burying of cables and pipelines, etc. Dorst et al., 2011). However, a disadvantage of the present model is its high computation times, which limits its utility for potential applications. This is because 3D simulations could be carried out on a single core. In future studies, other complex models (e.g., Delft3D Flexible Mesh, ROMS, MIKE 3, TELEMAC) could be used, which can run on multiple cores and thus have much shorter computation times.

5. Conclusions

In order to quantify and understand observed changes in 3D characteristics of offshore tidal sand waves under decreased sediment supply conditions, simulations were conducted with a 3D state-of-the-art numerical morphodynamic model. Overall, model simulates sand waves with characteristics that resemble those of observed sand waves. Sand waves that develop under sediment-starved conditions are more 3D, having isolated and more irregular crestlines, and which have larger spacings between successive crests (measured in the direction of the main depth-averaged tidal current). Their heights are lower compared with those in the case of sufficient supply. It was further found that sand waves migrate faster with decreasing sediment supply, an outcome that needs verification by further analysis of observed sand waves.

Declaration of Competing Interest

The authors declare that they have no known competing financial interests or personal relationships that could have appeared to influence the work reported in this paper.

Data availability

Model version, input files and output data used for this research can be accessed online on https://figshare.com/s/481214831abec0330840, while the Matlab scripts are available on https://figshare.com/s/f46a09d8c8af019f3784.

Acknowledgement

This research is part of NWO project NWA.ID.17.038 of the Netherlands Organisation of Scientific Research.

References

Besio, G., Blondeaux, P., Brocchini, M., Hulscher, S.J.M.H., Idier, D., Knaapen, M.A.F., Németh, A.A., Roos, P.C., Vittori, G., 2008. The morphodynamics of tidal sand waves: a model overview. Coast. Eng. 55, 657–670. https://doi.org/10.1016/j.coastaleng.2007.11.004.

Blondeaux, P., Vittori, G., Mazzuoli, M., 2016. Pattern formation in a thin layer of sediment. Mar. Geol. 376, 39–50. https://doi.org/10.1016/j.margeo.2016.03.011.

Campmans, G.H.P., Roos, P.C., Schrijen, E.P.W.J., Hulscher, S.J.M.H., 2018a. Modeling wave and wind climate effects on tidal sand wave dynamics: a North Sea case study. Estuar. Coast. Shelf Sci. 213, 137–147. https://doi.org/10.1016/j.ecss.2018.08.015.

Campmans, G.H.P., Roos, P.C., de Vriend, H.J., Hulscher, S.J.M.H., 2018b. The influence of storms on sand wave evolution: a nonlinear idealized modeling approach. J. Geophys. Res. Earth 123, 2070–2086. https://doi.org/10.1029/2018JF004616.

Carling, P.A., Golz, E., Orr, H.G., Radecki-Pawlik, A., 2000. The morphodynamics of fluvial sand dunes in the River Rhine, near Mainz, Germany. I. Sedimentology and morphology. Sedimentology 47, 227–252. https://doi.org/10.1046/j.1365-3091.2000.00290.x.

Creane, S., Coughlan, M., O'Shea, M., Murphy, J., 2022. Development and dynamics of sediment waves in a complex morphological and tidal dominant system: southern Irish Sea. Geosciences 12. https://doi.org/10.3390/geosciences12120431.

Damen, J.M., van Dijk, T.A.G.P., Hulscher, S.J.M.H., 2018. Spatially varying environmental properties controlling observed sand wave morphology. J. Geophys. Res. Earth 123, 262–280. https://doi.org/10.1002/2017JF004322.

Damveld, J.H., Borsje, B.W., Roos, P.C., Hulscher, S.J.M.H., 2020. Biogeomorphology in the marine landscape: Modelling the feedbacks between patches of the polychaete worm *Lanice conchilega* and tidal sand waves. Earth Surf. Process. Landf. 45, 2572–2587. https://doi.org/10.1002/esp.4914.

Dorst, L.L., Roos, P.C., Hulscher, S.J.M.H., 2011. Spatial differences in sand wave dynamics between the Amsterdam and the Rotterdam region in the Southern North Sea. Cont. Shelf Res. 31, 1096–1105. https://doi.org/10.1016/j.csr.2011.03.015.

Duffy, G.P., Hughes-Clarke, J.E., 2005. Application of spatial cross correlation to detection of migration of submarine sand dunes. J. Geophys. Res. Earth 110. https://doi.org/10.1029/2004JF000192.

Flemming, B.W., 1980. Sand transport and bedform patterns on the continental shelf between Durban and Port Elizabeth (southeast African continental margin). Sediment. Geol. 26, 179–205. https://doi.org/10.1016/0037-0738(80)90011-1.

Katoh, K., Kume, H., Kuroki, K., Hasegawa, J., 1998. The development of sand waves and the maintenance of navigation channels in the Bisanseto Sea, pp. 3490–3502. https://doi.org/10.1061/9780784404119.265.

Kleinhans, M.G., Wilbers, A.W.E., De Swaaf, A., Van Den Berg, J.H., 2002. Sediment supply-limited bedforms in sand-gravel bed rivers. J. Sediment. Res. 72, 629–640. https://doi.org/10.1306/030702720629.

Krabbendam, J.M., Nnafie, A., de Swart, H.E., Borsje, B., Perk, L., 2021. Modelling the past and future evolution of tidal sand waves. J. Mar. Sci. Eng. 9 https://doi.org/10.3390/jmse9101071.

Krabbendam, J.M., Roche, M., Van Lancker, V.R.M., Nnafie, A., Terseleer, N., Degrendele, K., De Swart, H.E., 2022. Do tidal sand waves always regenerate after dredging? Mar. Geol. 451, 106866. https://doi.org/10.1016/j.margeo.2022.106866.

Le Bot, S., Trentesaux, A., 2004. Types of internal structure and external morphology of submarine dunes under the influence of tide- and wind-driven processes (Dover Strait, northern France). Mar. Geol. 211, 143–168. https://doi.org/10.1016/j.margeo.2004.07.002.

Lesser, G.R., Roelvink, J.A., Van Kester, J.A.T.M., Stelling, G.S., 2004. Development and validation of a three-dimensional morphological model. Coast. Eng. 51, 883–915. https://doi.org/10.1016/j.coastaleng.2004.07.014.

Leuven, J.R.F.W., Kleinhans, M.G., 2019. Incipient tidal bar and sill formation. J. Geophys. Res. Earth 124, 1762–1781. https://doi.org/10.1029/2018JF004953.

Lobo, F.J., Hernández-Molina, F.J., Somoza, L., Rodero, J., Maldonado, A., Barnolas, A., 2000. Patterns of bottom current flow deduced from dune asymmetries over the Gulf of Cadiz shelf (Southwest Spain). Mar. Geol. 164, 91–117. https://doi.org/10.1016/S0025-3227(99)00132-2.

Ma, X., Yan, J., Song, Y., Liu, X., Zhang, J., Traykovski, P.A., 2019. Morphology and maintenance of steep dunes near dune asymmetry transitional areas on the shallow shelf (Beibu Gulf, northwest South China Sea). Mar. Geol. 412, 37–52. https://doi.org/10.1016/j.margeo.2019.03.006.

McCave, I.N., 1971. Sand waves in the North Sea off the coast of Holland. Mar. Geol. 10, 199–225. https://doi.org/10.1016/0025-3227(71)90063-6.

Netherlands Hydrographic Service, Royal Netherlands Navy, 2017. https://english.defensie.nl/organisation/navy/navy-units/hydrographic-service.

Núñez-González, F., Hesse, D., Ettmer, B., Gutierrez, R.R., Link, O., 2021. Development and validation of a novel metric for describing the three-dimensionality of bed forms. Geomorphology 390, 107856. https://doi.org/10.1016/j.geomorph.2021.107856.

Porcile, G., Blondeaux, P., Vittori, G., 2017. On the formation of periodic sandy mounds. Cont. Shelf Res. 145, 68–79. https://doi.org/10.1016/j.csr.2017.07.011.

Porcile, G., Blondeaux, P., Colombini, M., 2020. Starved versus alluvial river bedforms: an experimental investigation. Earth Surf. Process. Landf. 45, 1229–1239. https://doi.org/10.1002/esp.4800.

Porcile, G., Damveld, J.H., Roos, P.C., Blondeaux, P., Colombini, M., 2023. Modeling the genesis of sand-starved dunes in steady currents. J. Geophys. Res. Earth Surf. 128, e2022JF006796 https://doi.org/10.1029/2022JF006796.

Rubin, D.M., 2012. A unifying model for planform straightness of ripples and dunes in air and water. Earth Sci. Rev. 113, 176–185. https://doi.org/10.1016/j.earscirev.2012.03.010.

Tambroni, N., Bolla Pittaluga, M., Seminara, G., 2005. Laboratory observations of the morphodynamic evolution of tidal channels and tidal inlets. J. Geophys. Res. Earth 110. https://doi.org/10.1029/2004JF000243.

Tuijnder, A.P., Ribberink, J.S., Hulscher, S.J.M.H., 2009. An experimental study into the geometry of supply-limited dunes. Sedimentology 56, 1713–1727. https://doi.org/10.1111/j.1365-3091.2009.01054.x.

Van der Meijden, R., Damveld, J.H., Ecclestone, D.W., Van der Werf, J.J., Roos, P.C., 2023. Shelf-wide analyses of sand wave migration using GIS: a case study on the Netherlands continental shelf. Geomorphology 424, 108559. https://doi.org/10.1016/j.geomorph.2022.108559.

Van Gerwen, W., Borsje, B.W., Damveld, J.H., Hulscher, S.J.M.H., 2018. Modelling the effect of suspended load transport and tidal asymmetry on the equilibrium tidal sand wave height. Coast. Eng. 136, 56–64. https://doi.org/10.1016/j.coastaleng.2018.01.006.

Van Landeghem, K.J., Uehara, K., Wheeler, A.J., Mitchell, N.C., Scourse, J.D., 2009. Post-glacial sediment dynamics in the Irish Sea and sediment wave morphology: Data–model comparisons. Cont. Shelf Res. 29, 1723–1736. https://doi.org/10.1016/j.csr.2009.05.014.

Van Rijn, L.C., 1993. Principles of Sediment Transport in Rivers, Estuaries and Coastal Seas. Aqua Publications Amsterdam.

Van Veen, J., 1935. Sand waves in the North Sea. Int. Hydrograph. Rev. 12, 21–29.
Zhou, J., Wu, Z., Zhao, D., Guan, W., Cao, Z., Wang, M., 2022. Effect of topographic background on sand wave migration on the eastern Taiwan Banks. Geomorphology 398, 108030. https://doi.org/10.1016/j.geomorph.2021.108030.
Zijl, F., Sumihar, J., Verlaan, M., 2015. Application of data assimilation for improved operational water level forecasting on the northwest European shelf and North Sea. Ocean Dyn. 65, 1699–1716. https://doi.org/10.1007/s10236-015-0898-7.